

# First positronium imaging using $^{44}\text{Sc}$ with the J-PET scanner: a case study on the NEMA-Image Quality phantom

Manish Das, Sushil Sharma, Aleksander Bilewicz, Jarosław Choński, Neha Chug, Catalina Curceanu, Eryk Czerwiński, Jakub Hajduga, Sharareh Jalali, Krzysztof Kacprzak, Tefvik Kaplanoglu, Łukasz Kapłon, Kamila Kasperska, Aleksander Khreptak, Grzegorz Korcyl, Tomasz Kozik, Karol Kubat, Deepak Kumar, Anoop Kunimmal Venadan, Edward Lisowski, Filip Lisowski, Justyna Medrala-Sowa, Simbarashe Moyo, Wiktor Mryka, Szymon Niedźwiecki, Piyush Pandey, Szymon Parzych, Alessio Porcelli, Bartłomiej Rachwał, Elena Perez del Rio, Martin Rädler, Axel Rominger, Kuangyu Shi, Magdalena Skurzok, Anna Stolarz, Tomasz Szumlak, Pooja Tanty, Keyvan Tayefi Ardebili, Satyam Tiwari, Kavya Valsan Eliyan, Rafał Walczak, Ermias Yitayew Beyene, Ewa Ł. Stępień and Paweł Moskal

**Abstract**—Positronium Lifetime Imaging (PLI), an emerging extension of conventional positron emission tomography (PET) imaging, offers a novel window for probing the submolecular properties of biological tissues by imaging the mean lifetime of the positronium atom. Currently, the method is under rapid development in terms of reconstruction and detection systems. Recently, the first in vivo PLI of the human brain was performed using the J-PET scanner utilizing  $^{68}\text{Ga}$  isotope. However, this isotope has limitations due to its comparatively low prompt gamma yields, which is crucial for positronium lifetime measurement. Among alternative radionuclides,  $^{44}\text{Sc}$  stands out as a promising isotope for PLI, characterized by a clinically suitable half-life (4.04 hours) emitting 1157 keV prompt gamma in 100% cases

after the emission of the positron. This study reports the first experimental demonstration of PLI with  $^{44}\text{Sc}$ , carried out on a NEMA-Image Quality (IQ) phantom using the Modular J-PET tomograph—the first plastic scintillators-based PET scanner.

**Index Terms**—Positronium Lifetime Imaging, PET, NEMA,  $^{44}\text{Sc}$ , J-PET, Medical imaging, Positronium imaging.

## I. INTRODUCTION

**P**OSITRON Emission Tomography (PET) is an advanced nuclear imaging modality enabling the quantitative assessment of physiological and biochemical processes in vivo by detecting pairs of coincident gamma photons produced during positron-electron annihilation events [1], [2]. Recently, the method of positronium imaging was invented [3], [4] that enables imaging of positronium properties during the PET diagnosis. In the first clinical studies, the images of the mean positronium lifetime were demonstrated using the multi-photon J-PET scanner [5]. Next, positronium lifetime measurements were performed using Biograph Vision Quadra for reference materials [6] and humans [7].

Positronium Lifetime Imaging (PLI), relies on the fact that, in the human body, in almost 40% of cases, a metastable bound state (positronium atom, Ps) is formed. It consists of a positron emitted from an administered radiopharmaceutical and an electron from its molecular environment. Ps can be formed in one of the two spin configurations: para-positronium (pPs) or ortho-positronium (oPs), and according to spin-statistics, it is produced in a 1:3 ratio [8]. In the vacuum, the mean lifetime of oPs is equal to 142 ns, however, it is shortened to a few nanoseconds (1.4 to 2.9 ns [9]–[17]) within the environment of biological tissues, reflecting its sensitivity to the local molecular environment [18]. This observation advocates that imaging the Ps lifetime could serve as a novel biomarker for probing the submolecular characteristics and, potentially, for disease characterization at the submolecular level [16]. Therefore, PLI stands as a new method that may provide additional information in comparison to conventional PET/CT scans [4].

The oPs produced within tissue can be influenced due to the onset of several mechanisms leading to the shortening of its lifetime. One of such mechanisms is known as the pick-off

Manuscript received xxxx; revised xxxx; accepted xxxx. Date of publication xxxx; date of current version xxxx. We acknowledge support from the National Science Centre of Poland through grants MAE-STRO no. 2021/42/A/ST2/00423 (P.M.), OPUS no. 2021/43/B/ST2/02150 (P.M.), OPUS24+LAP no. 2022/47/I/ NZ7/03112 (E.S.) and SONATA no. 2023/50/E/ST2/00574 (S.S.), the Ministry of Science and Higher Education through grant no. IAL/SP/596235/2023 (P.M.), the SciMat and qLife Priority Research Areas budget under the program Excellence Initiative – Research University at Jagiellonian University (P.M. and E.S.), the Research Support Module as part of the Excellence Initiative – Research University program at Jagiellonian University (M.D.). We also acknowledge Polish high-performance computing infrastructure PLGrid (HPC Center: ACK Cyfronet AGH) for providing computer facilities and support within computational grant no. PLG/2024/017688.

(Corresponding authors: Manish Das: manish.das@doctoral.uj.edu.pl, Paweł Moskal: p.moskal@uj.edu.pl)

Manish Das, Sushil Sharma, Neha Chug, Eryk Czerwiński, Sharareh Jalali, Krzysztof Kacprzak, Tefvik Kaplanoglu, Łukasz Kapłon, Kamila Kasperska, Aleksander Khreptak, Grzegorz Korcyl, Tomasz Kozik, Karol Kubat, Deepak Kumar, Anoop Kunimmal Venadan, Justyna Medrala-Sowa, Simbarashe Moyo, Wiktor Mryka, Szymon Niedźwiecki, Piyush Pandey, Szymon Parzych, Alessio Porcelli, Elena Perez del Rio, Martin Rädler, Magdalena Skurzok, Pooja Tanty, Keyvan Tayefi Ardebili, Satyam Tiwari, Kavya Valsan Eliyan, Ermias Yitayew Beyene, Ewa Ł. Stępień and Paweł Moskal are with the Marian Smoluchowski Institute of Physics and the Center for Theranostics, Jagiellonian University, 31-007 Kraków, Poland

Aleksander Bilewicz and Rafał Walczak are with the Institute of Nuclear Chemistry and Technology, Warsaw, Poland.

Jarosław Choński and Anna Stolarz are with Heavy Ion Laboratory, University of Warsaw, Warsaw, Poland.

Catalina Curceanu is with INFN, Laboratori Nazionali di Frascati CP 13, Via E. Fermi 40, 00044, Frascati, Italy.

Jakub Hajduga, Bartłomiej Rachwał, Tomasz Szumlak are with AGH University of Science and Technology, Poland

Edward Lisowski and Filip Lisowski are with Cracow University of Technology, 31-864 Kraków, Poland.

Axel Rominger and Kuangyu Shi are with the Department of Nuclear Medicine, Inselspital, Bern University Hospital, University of Bern, 3010, Bern, Switzerland

process, in which the Ps picks-off an  $e^-$  from the surroundings and annihilates, mainly into two-photons [19]. Another dominant mechanism is due to the presence of oxygen molecules ( $O_2$ ) in tissues. The lifetime of oPs is reduced either by spin-exchange with paramagnetic ( $O_2$ ), flipping oPs into pPs which rapidly annihilates or through the oxidation under reactive oxidizing environments (e.g., presence of free radicals) where oPs undergoes an electron transfer reaction [18], [20].

Several research groups have conducted feasibility studies to explore the clinical use of PLI as reported in [5]–[7], [10], [21]–[32]. A PET scan detects 511 keV photon pairs that stem from both direct positron annihilations and Ps formation annihilations, but the latter have not been fully explored. In a conventional scanner, the detection time of annihilation photons gives an estimate of Ps decay time but determining its lifetime requires information about when Ps was formed. A positron-emitting ( $\beta^+$ ) source with an immediate prompt gamma release after  $\beta^+$  decay can meet this requirement.

In physics experiments,  $^{22}\text{Na}$  is the isotope of choice, e.g. for fundamental symmetries in the decays of Ps atoms [33]–[35]. The  $^{22}\text{Na}$  emits a 1275 keV prompt gamma ray in almost every  $\beta^+$  decay (99.94% branching ratio), thus providing a one-to-one coincidence between positron emission and prompt gamma release, where the prompt gamma marks the formation time of Ps. This intrinsic timing marker makes  $^{22}\text{Na}$  well suited for in-vitro and ex-vivo positronium lifetime studies in the laboratory [9]–[17]. The J-PET collaboration used this capability to conduct an ex vivo investigation of human cardiac myxoma and adipose tissues by placing  $^{22}\text{Na}$  source between each of these samples and measuring the oPs mean lifetimes. The results showed significant differences between myxoma at 1.9 ns and fat at 2.6 ns thus proving PLI's ability to detect variations in biological tissues [10], [16]. However,  $^{22}\text{Na}$  cannot be used for imaging of humans due to its long half-lifetime of 2.60 years and uptake in bones [36].

In general, multiple obstacles emerge when moving from controlled ex-vivo measurements to in-vivo studies because physiological motion, tissue heterogeneity, and background activity make precise lifetime determination challenging. The implementation of in vivo PLI requires a PET system with subnanosecond time-of-flight resolution, and a radionuclide with high branching ratio for  $\beta^+$  decay followed by the emission of prompt gamma. In addition, the radionuclide must have a suitable half-life for clinical use and must be manufactured through standard protocols (see Refs. [26], [37]).

In the first clinical trial, J-PET performed human brain PLI using  $^{68}\text{Ga}$ -PSMA, demonstrating the clinical potential of PLI through successful in-vivo mean lifetime imaging of oPs [5]. Despite these advances with  $^{68}\text{Ga}$  radionuclide, the fact that in only 1.34% of cases the prompt gamma ray accompanies the 511 keV photons imposes a major limitation for PLI.

In contrast,  $^{44}\text{Sc}$  emerges as the best potential candidate for PLI [38] with a favorable decay profile: a clinically compatible half-life of 4.04 h [39], an ultrashort de-excitation delay of 2.61 ps, and 100% decay producing a single, high-energy (1157 keV) prompt gamma after emission of positron [26]. This corresponds to a prompt gamma yield accompanied with the positron emission roughly 75 times greater than that of

$^{68}\text{Ga}$  [26]. The decay scheme of  $^{44}\text{Sc}$  is shown in Fig. 1(A). Although the medical application of  $^{44}\text{Sc}$  has not yet been established in clinical practice, its potential has been studied in detail in both the preclinical and clinical settings [39]–[48]. The performance of PET imaging using  $^{44}\text{Sc}$  has been shown through phantom studies [49], comparative evaluations of radionuclides [50], and preclinical radiotheranostic applications [51], [52]. In addition, first-in-human trials have shown its applicability for imaging neuroendocrine tumors and prostate cancer [53]–[56] and production methods suitable for clinical translation have been optimized [57].

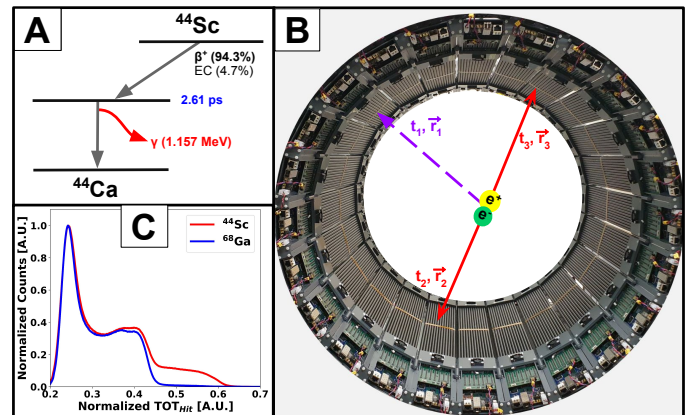


Fig. 1. (A) The decay schemes for the  $^{44}\text{Sc}$  isotope.  $\beta^+$  denotes the positron yield, EC indicates electron capture contributions, and  $\gamma$  represents the prompt gamma with energy indicated in the parenthesis. Additionally, the delay time is presented in blue text for clarity. The delay time denotes the average time between a positron's emission and a prompt gamma's emission. (B) The event definition of one prompt gamma ( $t_1, \vec{r}_1$ ) and two annihilation photons ( $(t_2, \vec{r}_2)$  and  $(t_3, \vec{r}_3)$ ) is depicted in the modular J-PET, requisite for positronium lifetime estimation. (C) Experimental Time-Over-Threshold (TOT) spectra for  $^{68}\text{Ga}$  and  $^{44}\text{Sc}$ , showing an increased prompt gamma yield for  $^{44}\text{Sc}$  in the modular J-PET scanner.

Presently, only four PET systems, the J-PET scanner in Cracow, Poland [5], the Biograph Vision Quadra in Bern, Switzerland [6], [7], [58], the PennPET Explorer in Philadelphia, USA [32], [59], [60], and the brain-dedicated TOF-PET scanner VRAIN in Chiba, Japan [30], [31]—are capable of measuring the lifetime of positronium. In recent years, several reconstruction algorithms for PLI have also been proposed [4], [22]–[25], [32], [61]–[65]. Recent investigations using the Biograph Vision Quadra [6], [7] have revealed energy-detection limits for high-energy prompt gammas. The system records photons below 950 keV but cannot resolve energy depositions above 726 keV. This results in many events being lost, and the imprecise identification of  $\gamma$ -rays can increase background counts. Although in the case of  $^{124}\text{I}$ , lower energy prompt gammas remain detectable, using  $^{68}\text{Ga}$  and  $^{44}\text{Sc}$  suffers substantial photon losses under these constraints. In contrast, the J-PET scanner, the PennPET Explorer and the brain-dedicated VRAIN system used for PLI [5], [30]–[32], [59], do not have this constraint of energy detection.

Fig. 1(B) shows the modular J-PET scanner [66], [67] which was used to demonstrate the first positronium images [5], [10]. This scanner was used in the study presented here.

Fig. 1(C) presents the experimental spectra of Time-Over-Threshold (TOT) values (which is a measure of the energy deposition [68]). One can see that for TOT values above 0.45, corresponding to the registration of prompt gamma, the signal for  $^{44}\text{Sc}$  is higher than that for  $^{68}\text{Ga}$ .

In this work, we present the first experimental demonstration of PLI with  $^{44}\text{Sc}$  carried out on a NEMA Image Quality phantom using the modular J-PET scanner [5], [38], which supports multiphoton detection without energy restrictions on deexcitation photons (Fig. 1C).

## II. METHODS

### A. Isotope preparation

In this study, two radionuclides emitting positrons were investigated: Fluorine-18 ( $^{18}\text{F}$ ) and Scandium-44 ( $^{44}\text{Sc}$ ). These isotopes exhibit different characteristics:  $^{18}\text{F}$  decays predominantly by  $\beta^+$  decay (97%) and, to a lesser extend, by electron capture (3%), without significant prompt gamma emission. In contrast,  $^{44}\text{Sc}$  undergoes  $\beta^+$  decay in approximately 94.3% and subsequently emits a 1157 keV prompt  $\gamma$ -ray with a yield of around 100% [26]. The inherited differences in the prompt gamma emission serve to demonstrate the effectiveness of the selection criteria developed to identify events having additional prompt gammas for PLI. Moreover, this approach can be extended for effective implementation of simultaneous imaging of double isotopes as described in [69], although this is beyond the scope of the presented work.

The  $^{18}\text{F}$  was purchased from the commercial supplier VOXEL and  $^{44}\text{Sc}$  was produced by the Heavy Ion Laboratory of the University of Warsaw [70]–[72] via the  $^{44}\text{Ca}(p,n)^{44}\text{Sc}$  reaction. A natural calcium carbonate target ( $\text{CaCO}_3$  tablets) was irradiated for 2 hours and 20 minutes using a 16.5 MeV proton beam with a current of 15  $\mu\text{A}$ . Each tablet weighed 70 mg and was pressed onto a black graphite pad, with a total weight of 342 mg per disc. After irradiation, the target disc was dissolved in diluted hydrochloric acid (HCl) to obtain a scandium solution. The solution was then filtered to remove graphite dust, separated, concentrated, and subsequently buffered to raise the pH from 0.5 to approximately 4.0.

### B. Phantom Study

The NEMA IQ Phantom (Pro-Project Pro-NM NEMA NU2) was used in the study, which comprises six spherical inserts of 10, 13, 17, 22, 28 and 37 mm diameter and a lung-equivalent insert filled with styrofoam balls. The background compartment of the phantom was filled with demineralized water and contained no radioactivity.

In the NEMA IQ phantom, shown in Fig. 2(A), spheres with diameters of 10 mm, 13 mm, and 17 mm were filled with  $^{18}\text{F}$ , while spheres with diameters of 22 mm, 28 mm, and 37 mm were filled with  $^{44}\text{Sc}$ , both mixed with water, at activity concentrations of 0.574 MBq/mL and 0.185 MBq/mL, respectively, measured at the start of the experiment. The phantom was then positioned inside the detector as shown in Fig. 2(B), and the data was acquired for a duration of 178 minutes.

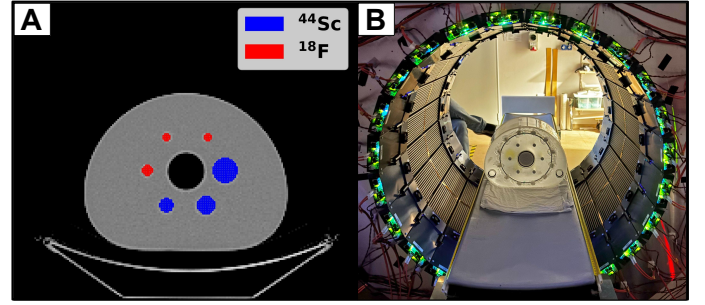


Fig. 2. (A) Transaxial CT scan of the NEMA IQ phantom schematically depicting the radiotracer distribution in the spheres, with those highlighted in red containing  $^{18}\text{F}$  and those in blue filled with  $^{44}\text{Sc}$ . (B) The NEMA IQ phantom positioned inside the modular J-PET detector.

### C. Event Selection for positronium imaging

The event selection criteria, established in our previous work [5], [10], provide a clear distinction between positronium-related signals and standard two-photon annihilation events used for standard PET imaging [5], [10]. The principle of standard PET relies on the detection in coincidence of two back-to-back 511 keV annihilation photons ( $\gamma_a$ ), while PLI requires both annihilation photons and a third additional prompt gamma ( $\gamma_p$ ) used as start signal for Ps formation. The J-PET scanner operates in trigger-less mode allowing multiphoton detection simultaneously. The data acquisition and signal processing methods used in J-PET are explained in [5], [73], [74].

In this work, we classified events into two categories based on the radionuclide type:  $^{18}\text{F}$  produces two back-to-back 511 keV photons, and  $^{44}\text{Sc}$  emits two 511 keV annihilation photons together with a 1157 keV prompt gamma ( $\gamma_p$ ). The primary interaction of incident photons in plastic scintillators occurs through Compton scattering depositing ranges of energies based on the scattering angle [75]. The TOT measurement in each scintillator strip is used to determine the incident photon energy deposition [68]. For a registered interaction (hit), the obtained TOT value results from averaging the TOT values measured from the matrix of Silicon Photomultipliers (SiPMs) attached at both ends of the scintillator and directly relates to the energy deposited by Compton-scattered photons. The measured TOT spectrum is shown in Figure 3(A). The Compton edges for 511 keV and 1157 keV photons appear at 7.5 ns.V and 11 ns.V, respectively. These values correspond to the maximum energy transfer during a single Compton scattering event. The TOT signal range from 5.5 to 8 ns.V is used to select 511 keV photons (red shaded area) and the TOT signal range from 8.1 to 14 ns.V identifies 1157 keV photons (blue shaded area). The formation of individual events relies on photon interactions (hits) that fall within a 20 ns coincidence window for both  $\gamma_a$  and  $\gamma_p$ . The selection criteria for 2-hit ( $2\gamma_a$ ) events, which require exactly two 511 keV hits, are explained in [76]. This work focuses on 3-hit ( $2\gamma_a + \gamma_p$ ) events from the perspective of PLI. However, the comparison between reconstructed images based on events with a multiplicity of 2 hits ( $2\gamma_a$ ) and 3-hits ( $2\gamma_a + \gamma_p$ ) are presented.

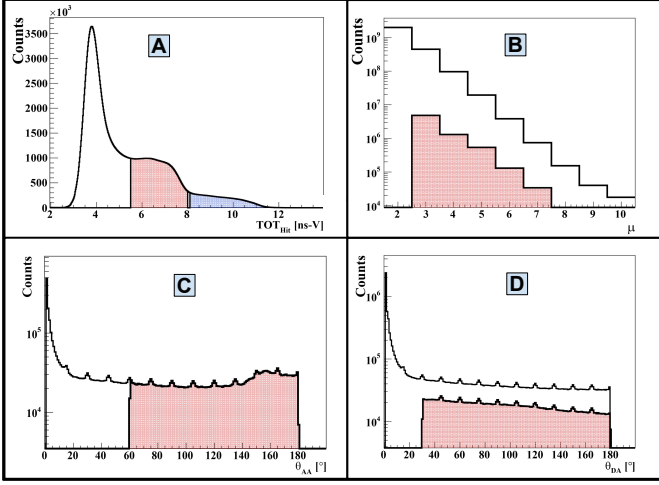


Fig. 3. (A) Distribution of time-over-threshold ( $TOT_{Hit}$ ) for photon identification, with annihilation photons (red) and prompt gammas (blue) marked by distinct ranges. (B) Hit multiplicity ( $\mu$ ) distribution, with a red-shaded histogram highlighting events containing one prompt gamma, and two annihilation photons. (C) Distribution of the relative angle ( $\theta_{AA}$ ) between annihilation photon vectors  $\vec{r}_2$  and  $\vec{r}_3$  (per Fig. 1B), with  $\theta_{AA} \geq 60^\circ$  (red) as the selection criterion. (D) Distribution of the relative angle ( $\theta_{DA}$ ) between prompt gamma vector  $\vec{r}_1$  and annihilation photon vectors  $\vec{r}_2, \vec{r}_3$  (per Fig. 1B), with  $\theta_{DA} \geq 30^\circ$  (red) as the restriction.

The next selection criterion is based on the event-wise hit multiplicity (Fig. 3(B)). For PLI with  $^{44}\text{Sc}$ , we require exactly three hits per event ( $\mu=3$ ): two corresponding to the 511 keV annihilation photons with  $TOT_{hit} \in [5.5 - 8]\text{ns} \cdot \text{V}$  and one corresponding to the 1157 keV prompt gamma with  $TOT_{hit} \in [8.1 - 14]\text{ns} \cdot \text{V}$ . The distribution of multiplicity of accepted events is shown in Fig. 3(B), where the red-shaded histogram highlights events containing exactly two annihilation photons and one prompt gamma.

To suppress the background from scattered photons or accidental coincidences, we imposed angular constraints on the emitting direction of photons. Fig.3(C) shows the distribution of the angle  $\theta_{AA}$  between the annihilation photons calculated from their hit positions with respect to the detector center. Only events with  $\theta_{AA}$  (red-shaded region in Fig.3(C)) were accepted for further analysis. Moreover, the prompt gamma  $\gamma_d$  is emitted isotropically with respect to the annihilation photons. However the observed distribution of the angle between the annihilation photons and prompt gamma is strongly peaked for small angles. This is due to the misidentification of secondary scattering of photons in the detector as signals from prompt gamma or annihilation photon. Therefore, the selected events were further reduced by implementing the additional constraint ( $\theta_{DA} \geq 30^\circ$ ) that significantly improved the purity of true event (Fig.3(D)).

Finally, we applied a Scatter Test (ST) to distinguish events with true annihilation photons from contamination by intra-detector Compton scatter or accidental coincidences. For annihilation photons registered with hit times  $t_2$  and  $t_3$ , and hit positions  $\vec{r}_2$  and  $\vec{r}_3$ , the ST is defined as

$$ST = |t_3 - t_2| - |\vec{r}_3 - \vec{r}_2|/c, \quad (1)$$

where  $c$  is the speed of light. In the ideal case of direct detection of annihilation photons ( $t_2 = t_3$ ), the value of ST is smaller than zero. In the case if the registered hits correspond to the primary and secondary scattering of the same photon, then  $ST = 0$  within the experimental resolution. For the accidental coincidences, the time difference between the hits  $|t_3 - t_2|$  may be large, yielding the ST value greater than zero. By selecting the annihilation pairs for which the ST value is less than ( $ST < -0.5$  ns) the purity of the selected events was enhanced.

#### D. Image reconstruction

The reconstruction of images was performed for both conventional PET ( $2\gamma_a$ ) and positronium ( $2\gamma_a + \gamma_p$ ) events, enabling a direct comparison between standard and Ps-enhanced modalities. It is worth mentioning that in both cases only annihilation pairs (511 keV) were used for image reconstruction. In the category of  $2\gamma_a + \gamma_p$  events, an additional prompt gamma ( $\gamma_p$ ) was included for subsequent lifetime analysis. The annihilation point  $\vec{r}_a$  and annihilation time  $t_a$  are calculated from the time and position of the annihilation hits ( $(t_2, \vec{r}_2)$  and  $(t_3, \vec{r}_3)$ ):

$$\vec{r}_a = \frac{\vec{r}_2 + \vec{r}_3}{2} + \frac{c(t_3 - t_2)}{2} \cdot \frac{\vec{r}_2 - \vec{r}_3}{|\vec{r}_2 - \vec{r}_3|}, \quad (2)$$

and

$$t_a = \frac{t_2 + t_3}{2} - \frac{|\vec{r}_2 - \vec{r}_3|}{2c}. \quad (3)$$

As the next step, the data acquired with J-PET were converted into a list-mode file using the J-PET framework for CASToR, an open-source reconstruction software [77]. The image reconstruction used the Maximum Likelihood Expectation Maximization (MLEM) algorithm, which ran for 10 iterations. The dimensions of the reconstructed image were established at  $200 \times 200 \times 200$  voxels, with each voxel having a size of  $2.5 \times 2.5 \times 2.5$  mm<sup>3</sup>. The reconstructed images were smoothed using a 5-mm Gaussian filter uniformly. The reconstructed images are shown in the results section.

#### E. Positronium Lifetime estimation

The emitted positrons in  $\beta^+$  decay can annihilate either by direct interaction with a surrounding electron ( $e^-$ ) – a process lasting on average about 388 ps [10] or by the formation of an  $e^+e^-$  bound state known as Ps. Ps can be produced in two distinct ground states: para-Ps (pPs), which has a mean lifetime of approximately 125 ps, and ortho-Ps (oPs), a longer-lived state with a mean lifetime in water of about 1.83 ns [78]. Consequently, the measured positron lifetime can vary depending on the annihilation mechanism. The positron lifetime, defined as  $\Delta T = t_a - t_p$ , represents the time difference between positron emission and its subsequent annihilation. Here,  $t_a$  denotes the positron annihilation time, while  $t_p$  approximates the positron emission time. In the  $^{44}\text{Sc}$  decay process, the prompt gamma is emitted on average 2.6 ps after the emission of the positron, according to its decay scheme presented in Fig. 1(A). Therefore, the prompt gamma emission time ( $t_p$ ) is used as an approximation for the positron

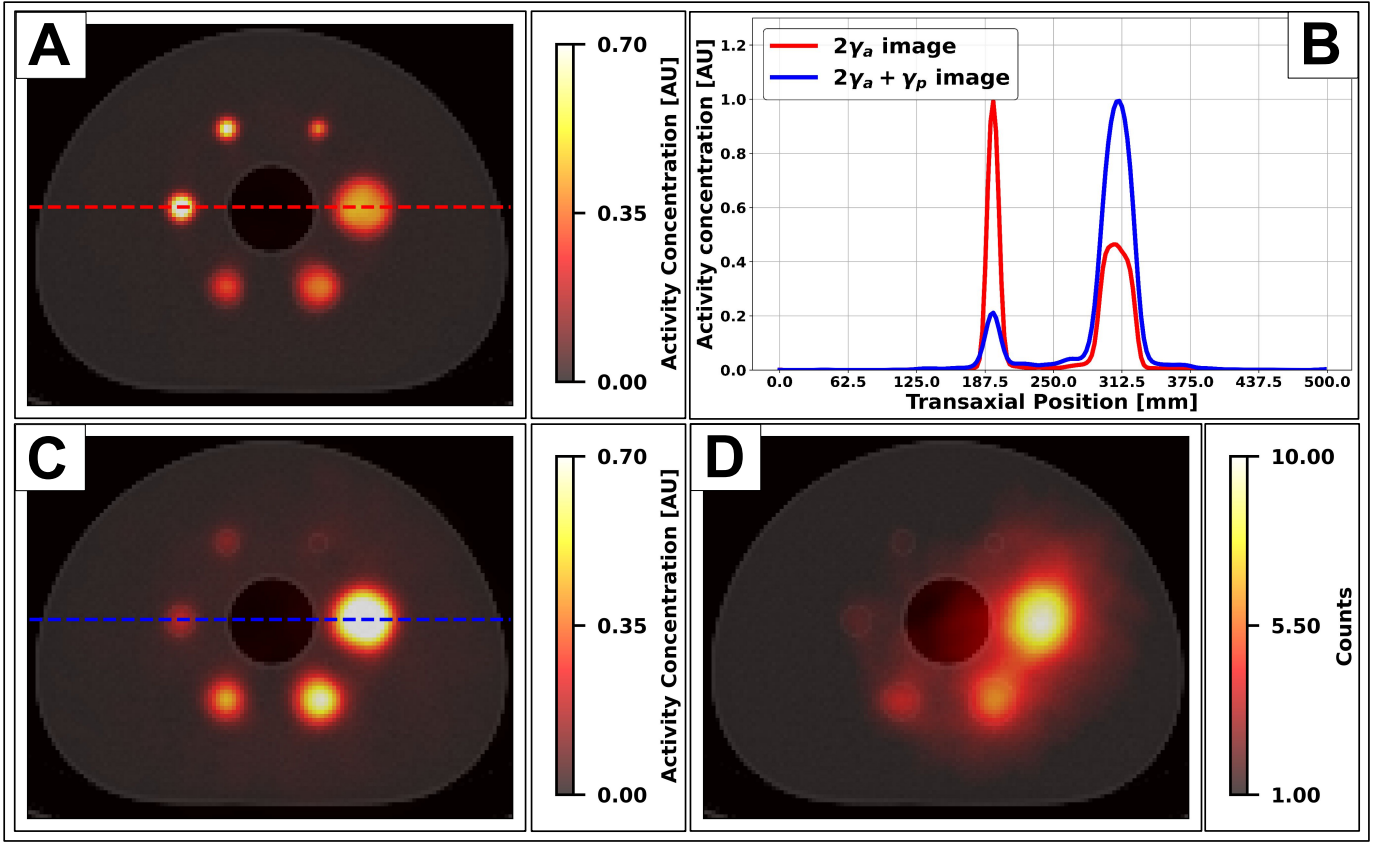


Fig. 4. (A) Transaxial view of the conventional PET image ( $2\gamma_a$ ) obtained from the modular J-PET, reconstructed with CASToR and overlaid on the CT image. (B) Line profile along the indicated dashed line in the images. The red line represents the profile for the conventional PET image, showing that the  $^{18}\text{F}$  activity concentration is more than two times higher than  $^{44}\text{Sc}$  along the image slice. The blue line corresponds to the  $2\gamma_a + \gamma_p$  image. (C) Transaxial view of the  $2\gamma_a$  image for  $2\gamma_a + \gamma_p$  events, reconstructed using two 511 keV photons in CASToR and overlaid on the CT image. (D) Transaxial view of the annihilation point distribution ( $\vec{r}_a$ ) overlaid on the CT image of the NEMA IQ phantom, with voxels having a relative intensity greater than 10% displayed.

emission time. The emission time is determined by subtracting the time of flight of prompt gamma from the time of its registration ( $t_1$ ):

$$t_p = t_1 - \frac{|\vec{r}_1 - \vec{r}_a|}{c}, \quad (4)$$

where  $\vec{r}_1$  is the registered hit position of prompt gamma and  $\vec{r}_a$  corresponds to the annihilation point reconstructed using Eq. 2. The short range of positrons from  $^{44}\text{Sc}$  supports our assumption that the prompt gamma originates from the annihilation site. The average distance between emission and annihilation is approximately 1.7 mm in tissues [26].

The measured  $\Delta T$  spectrum was analyzed by fitting a sum of exponential decay components convoluted with the experimental time resolution, using the dedicated PALS Avalanche software to estimate the mean oPs lifetime, as detailed in [10], [79]–[81]. The initial values for pPs and direct-annihilation contributions were set to a lifetime of 125 ps with 10% relative intensity and 388 ps with 60% intensity, respectively. To optimize the fitting results, both lifetimes and their intensities were permitted to vary up to 200% of the initial value. The background level was estimated by averaging the bin counts in the range of -10 ns to -5 ns and subtracted before the fitting. Three distinct fitting

approaches were used:

**Model 1 (Fixed Background):** maintained a constant background level at its pre-estimated value while allowing the oPs lifetime and intensity to vary freely.

**Model 2 (Constrained Background):** the background level was permitted to vary between  $-3\sigma$  to  $+3\sigma$  of its mean value where  $\sigma$  represents the standard deviation of the counts in the -10 ns to -5 ns interval. The oPs lifetime and intensity remained free. This method reduces bias and instability in low-statistics datasets through statistical fluctuation accommodation.

**Model 3 (Extended Parameter Range):** the background remained constant while the oPs lifetime and intensity were permitted to change within 200% of their initial values which were set to 2 ns and 30%, respectively.

In addition to the mean oPs lifetimes, the mean positron lifetime ( $\Delta T_{\text{mean}}$ ) in the signal region from 0 to 5 ns in the  $\Delta T$  spectrum was estimated after subtracting the background:

$$\Delta T_{\text{mean}} = \frac{\sum_{i=0}^{5 \text{ ns}} (N_i - N_b) \Delta T_i}{\sum_{i=0}^{5 \text{ ns}} (N_i - N_b)}, \quad (5)$$

where  $N_i$  is the number of events for  $\Delta T_i$  and  $N_b$  is the

number of background events estimated by averaging the bin counts in the range of -10 ns to -5 ns. The results of the estimated mean oPs lifetime ( $\tau_{\text{oPs}}$ ) and  $\Delta T_{\text{mean}}$  are presented in the Results III section.

### III. RESULTS

The transaxial view of the MLEM reconstructed conventional PET ( $2\gamma_a$ ) image, obtained with the J-PET scanner using the parameters described in the Methods section, is shown in Fig. 4(A). The image is corrected for sensitivity, attenuation, and normalization (see [76] for details). The effective activity concentration ratio in the reconstructed image, initially 3.10 for  $^{18}\text{F}$  to  $^{44}\text{Sc}$ , should be approximately 2.38 after a 178 minute acquisition due to the different isotopes' decay rates. This ratio reflects the time-integrated activities, calculated using decay constants of  $0.006316 \text{ min}^{-1}$  for  $^{18}\text{F}$  and  $0.002909 \text{ min}^{-1}$  for  $^{44}\text{Sc}$  over 178 minutes. The line profile shown in Fig. 4(B) for the  $2\gamma_a$  image indicates that the ratio of the maximum activity concentrations between  $^{18}\text{F}$  and  $^{44}\text{Sc}$  in the given image slice is approximately 2.08.

Next, the reconstructed  $2\gamma_a + \gamma_p$  image using CASToR is shown in Fig.4(C), demonstrating the effectiveness of the selection criteria. The line profile along the 17 mm and 37 mm diameter spheres [Fig.4(B)] shows that events from  $^{18}\text{F}$  are significantly reduced, as  $^{18}\text{F}$  releases almost no prompt gammas associated with positron emission. The remaining  $^{18}\text{F}$  events could be attributed to the possibility of detecting a prompt gamma from  $^{44}\text{Sc}$  while registering two annihilation photons from  $^{18}\text{F}$  within the 20 ns event time window, which introduces false  $2\gamma_a + \gamma_p$  events in  $^{18}\text{F}$ , primarily contributing to the background.

Furthermore, the obtained annihilation position ( $r_a^-$ ) [Eq. 2] is shown in Fig. 4(D). The image clearly shows high counts in the spheres measuring 22 mm, 28 mm, and 37 mm in diameter, which were filled with  $^{44}\text{Sc}$ . The positron lifetime ( $\Delta T$ ) values for each sphere were extracted by defining regions of interest (ROIs) within the different spheres, as shown in Fig. 5(A), and were plotted using a bin width of 100 ps.

The body and spheres in the NEMA-IQ phantom are made of PMMA (polymethyl methacrylate), and the oPs lifetime in PMMA ranges from approximately 1.7 ns to 1.9 ns, depending on the temperature ( $20^\circ\text{C}$  to  $60^\circ\text{C}$ ) [82]. This range is comparable to the oPs lifetime in water, which is approximately  $1.839 \pm 0.015 \text{ ns}$  at  $20^\circ\text{C}$  [78]. Therefore, the contributions of oPs lifetime in water and PMMA were combined as a single component in the fitting procedure.

The results from the fit are presented in Table I for the different fitting models. In Fitting Model 1, the mean oPs ( $\tau_{\text{oPs}}$ ) lifetime in the 28 mm, 37 mm, and 22 mm diameter spheres is shown in Fig. 5(B-E). The mean oPs lifetime in the 28 mm and 37 mm spheres is in excellent agreement with the mean oPs lifetime in water ( $1.839 \pm 0.015 \text{ ns}$  [78]), while the mean oPs lifetime in the 22 mm sphere is  $1.413 \pm 0.070 \text{ ns}$ . This discrepancy could be attributed to several factors: the number of events from this sphere was lower compared to the others, and the background might have been overestimated. To address this, in Fitting Model 2, the background level was allowed to

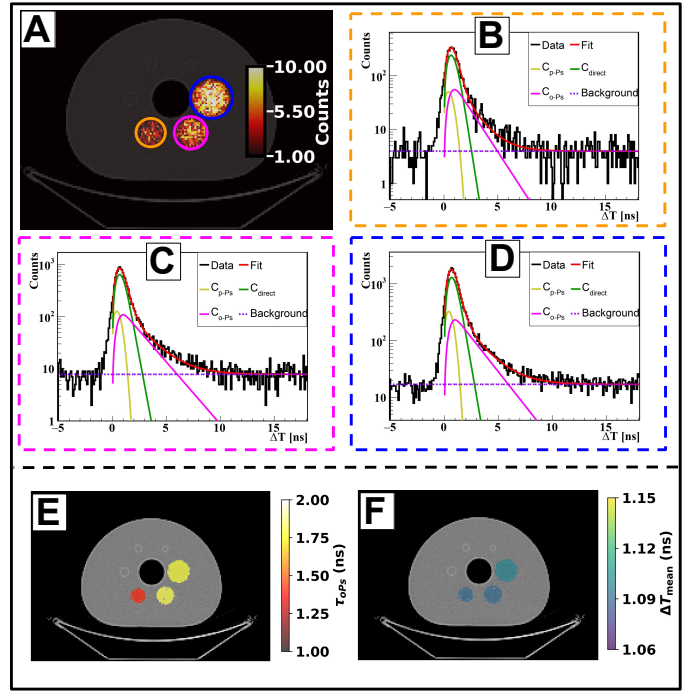


Fig. 5. (A) Transaxial view of the NEMA-IQ phantom with selected ROIs from the spheres, overlaid on the CT image of the NEMA IQ phantom. (B–D) Distributions of positron annihilation lifetimes ( $\Delta T$ ) for the 22 mm (B), 28 mm (C), and 37 mm (D) diameter spheres. The black histograms represent the experimental data, while the overlaid curves correspond to the fitted components: pPs ( $C_{\text{pPs}}$ ), direct annihilations ( $C_{\text{direct}}$ ), oPs ( $C_{\text{oPs}}$ ), and background from accidental coincidences. The red curve represents the total fit, obtained as the sum of all contributions. (E–F) Visualization of the estimated mean oPs lifetime ( $\tau_{\text{oPs}}$ ) (E) and mean positron lifetime ( $\Delta T_{\text{mean}}$ ) (F) from Fitting Model 1, where the activity counts within each selected ROI are replaced by their respective lifetime values.

vary within  $\pm 3\sigma$  of its estimated mean, which resulted in a mean lifetime in the smallest sphere that was more consistent with the oPs lifetime in water.

In Fitting Model 3, where all parameters were free within selected limits, the lifetime values remained consistent with those obtained from Fitting Model 1. Beyond these observations, the mean positron lifetime ( $\Delta T_{\text{mean}}$ ) proved to be a more robust parameter for lifetime characterization, as previously demonstrated [5]. Notably,  $\Delta T_{\text{mean}}$  showed consistent results within 10 ps across all fitting models, regardless of the variations in the mean oPs lifetime (as shown in Fig. 5(F) for Fitting Model 1).

### IV. DISCUSSION

In this study, we performed the first PLI with the  $^{44}\text{Sc}$  using the modular J-PET scanner. The results show that  $^{44}\text{Sc}$  is a suitable radionuclide for PLI because it emits prompt gamma (1157 keV) after the emission of positron in almost 100% cases, and has a half-life of 4.04 hours [39]. We measured oPs lifetimes in the spheres of the NEMA IQ phantom, where the mean oPs lifetime value in the two largest spheres of the phantom matches with the reported value in water [78]. However, the results from the smallest sphere measurements highlight the statistical limitations and inaccuracies in the measurement of background estimation. In the analysis, we

TABLE I

POSITRONIUM LIFETIME AND INTENSITY OBTAINED FROM FITTING THE POSITRON LIFETIME SPECTRA USING THREE DIFFERENT MODELS.  $D$  REPRESENTS THE DIAMETER OF THE SPHERES.  $\tau_{\text{OPs}}$  IS THE MEAN LIFETIME OF OPS.  $I_{\text{OPs}}$ ,  $I_{\text{DIRECT}}$ , AND  $I_{\text{PPs}}$  ARE THE RELATIVE INTENSITIES CORRESPONDING TO OPS ANNIHILATION, DIRECT POSITRON-ELECTRON ANNIHILATION, AND PPS ANNIHILATION, RESPECTIVELY.  $\Delta T_{\text{mean}}$  DENOTES THE MEAN POSITRON LIFETIME.

| Fitting Model 1 |                          |                      |                         |                      |                               |
|-----------------|--------------------------|----------------------|-------------------------|----------------------|-------------------------------|
| $D$ [mm]        | $\tau_{\text{OPs}}$ [ns] | $I_{\text{OPs}}$ [%] | $I_{\text{direct}}$ [%] | $I_{\text{PPs}}$ [%] | $\Delta T_{\text{mean}}$ [ns] |
| 22.00           | $1.413 \pm 0.070$        | $28.46 \pm 1.26$     | $61.11 \pm 1.43$        | $10.43 \pm 1.20$     | $1.099 \pm 0.013$             |
| 28.00           | $1.821 \pm 0.061$        | $25.55 \pm 0.74$     | $63.41 \pm 0.89$        | $11.04 \pm 0.73$     | $1.099 \pm 0.008$             |
| 37.00           | $1.804 \pm 0.042$        | $25.84 \pm 0.52$     | $62.05 \pm 0.63$        | $12.10 \pm 0.52$     | $1.102 \pm 0.005$             |
| Fitting Model 2 |                          |                      |                         |                      |                               |
| $D$ [mm]        | $\tau_{\text{OPs}}$ [ns] | $I_{\text{OPs}}$ [%] | $I_{\text{direct}}$ [%] | $I_{\text{PPs}}$ [%] | $\Delta T_{\text{mean}}$ [ns] |
| 22.00           | $1.693 \pm 0.087$        | $25.68 \pm 1.13$     | $56.96 \pm 1.38$        | $17.36 \pm 1.16$     | $1.122 \pm 0.013$             |
| 28.00           | $2.129 \pm 0.076$        | $23.43 \pm 0.70$     | $63.99 \pm 0.88$        | $12.58 \pm 0.71$     | $1.108 \pm 0.008$             |
| 37.00           | $1.836 \pm 0.044$        | $25.40 \pm 0.51$     | $62.62 \pm 0.62$        | $11.98 \pm 0.51$     | $1.102 \pm 0.005$             |
| Fitting Model 3 |                          |                      |                         |                      |                               |
| $D$ [mm]        | $\tau_{\text{OPs}}$ [ns] | $I_{\text{OPs}}$ [%] | $I_{\text{direct}}$ [%] | $I_{\text{PPs}}$ [%] | $\Delta T_{\text{mean}}$ [ns] |
| 22.00           | $1.398 \pm 0.068$        | $29.13 \pm 1.23$     | $62.85 \pm 1.38$        | $8.02 \pm 1.04$      | $1.099 \pm 0.013$             |
| 28.00           | $1.815 \pm 0.008$        | $25.68 \pm 0.73$     | $65.15 \pm 0.89$        | $9.17 \pm 0.70$      | $1.099 \pm 0.008$             |
| 37.00           | $1.838 \pm 0.044$        | $25.23 \pm 0.50$     | $65.07 \pm 0.60$        | $9.71 \pm 0.43$      | $1.102 \pm 0.005$             |

used different fitting models to mitigate these problems, as the wrong background estimation strongly affects the stability and accuracy of the mean oPs lifetime measurement.

We observed that Fitting Model 2, with constrained background estimation, improved the consistency in mean oPs lifetime ( $\tau_{\text{OPs}}$ ) estimation for smaller volume, demonstrating the necessity of adaptive background handling to improve measurement accuracy.

Furthermore, it was found that the mean positron lifetime ( $\Delta T_{\text{mean}}$ ) is a more robust parameter within the 10 ps range across all fitting models, which proves its significance for PLI. The Modular J-PET system, built with cost-effective plastic scintillators [83], is a promising proof of concept for scalable, total-body PET and positronium imaging. It operates in triggerless mode, allowing simultaneous multi-photon detection, which is essential for accurate positronium lifetime measurements. New research demonstrates how  $^{44}\text{Sc}$  serves a dual purpose in theranostics through diagnostic imaging and targeted radiotherapy, which makes it an ideal choice for multiple applications [84], [85]. The combination of the suitability of  $^{44}\text{Sc}$  and the detection capability of modular J-PET establishes a strong experimental basis that may support the clinical and preclinical application of  $^{44}\text{Sc}$ -based PLI. Furthermore, the enhanced large axial field-of-view (LAFOV) of total body PET systems will improve the sensitivity several times for PLI [5], [38]. Therefore, the advancement of PLI will lead to a broader medical application, for instance, exploring its potential as a novel diagnostic indicator [5].

## V. CONCLUSION

In this study, we successfully demonstrated the feasibility of PLI using  $^{44}\text{Sc}$  with the Modular J-PET tomograph carried out with a NEMA IQ phantom. The promising results of this study mark an important step forward and open new possibilities for advancing PLI techniques. With the advent of total body PET

systems, PLI will become accessible through the enhancement of LAFOV scanners [6], [58], [86], [87] and hence the overall sensitivity of the scanner. Furthermore, the possibility of using the more enhanced and optimized reconstruction algorithm [22]–[25], [32], [62]–[65], will pave the way towards the application of PLI in clinical and preclinical scans.

## DECLARATIONS

Pawel Moskal is the inventor on a patent related to this work [patent nos.: (Poland) PL 227658, (Europe) EP 3039453, and (United States) US 9,851,456], filed (Poland) 30 August 2013, (Europe) 29 August 2014, and (United States) 29 August 2014; published (Poland) 23 January 2018, (Europe) 29 April 2020, and (United States) 26 December 2017. The authors declare that they have no other competing interests.

## REFERENCES

- [1] M. E. Phelps, "PET: The Merging of Biology and Imaging into Molecular Imaging," *Journal of Nuclear Medicine*, vol. 41, no. 4, pp. 661–681, 2000. [Online]. Available: <https://jnm.snmjournals.org/content/41/4/661>
- [2] A. Alavi, T. J. Werner, E. Ł. Stepień, and P. Moskal, "Unparalleled and revolutionary impact of PET imaging on research and day to day practice of medicine," *Bio-Algorithms and Med-Systems*, vol. 17, pp. 203–220, 2021.
- [3] P. Moskal, "Positronium imaging," in *2019 IEEE Nuclear Science Symposium and Medical Imaging Conference (NSS/MIC)*, 2019, pp. 1–3.
- [4] P. Moskal, A. Bilewicz, M. Das, B. Huang, A. Khreptak, S. Parzych, J. Qi, A. Rominger, R. Seifert, S. Sharma, K. Shi, W. Steinberger, R. Walczak, and E. Stepień, "Positronium Imaging: History, Current Status, and Future Perspectives," *IEEE Trans. Radiat. Plasma Med. Sci. (in print)*, 2025. [Online]. Available: <https://arxiv.org/abs/2503.14120>
- [5] P. Moskal, J. Baran, S. Bass, J. Choiński, N. Chug, C. Curceanu, E. Czerwiński, M. Dadgar, M. Das, K. Dulski, K. V. Eliyan, K. Fronczewska, A. Gajos, K. Kacprzak, M. Kajetanowicz, T. Kaplanoglu, Ł. Kapłon, K. Klimaszewski, M. Kobylecka, G. Korcyl, T. Kozik, W. Krzemień, K. Kubat, D. Kumar, J. Kunikowska, J. Mączewska, W. Migdał, G. Moskal, W. Mryka, S. Niedźwiecki, S. Parzych, E. P. del Rio, L. Raczyński, S. Sharma, S. Shivani, R. Y. Shopa, M. Silarski, M. Skurzok, F. Tayefi,

- K. T. Ardebili, P. Tanty, W. Wiślicki, L. Królicki, and E. Ł. Stępień, "Positronium image of the human brain in vivo," *Science Advances*, vol. 10, no. 37, p. eadp2840, 2024. [Online]. Available: <https://www.science.org/doi/abs/10.1126/sciadv.adp2840>
- [6] W. M. Steinberger, L. Mercolli, J. Breuer, G. Prenosil, K. Shi, A. Rominger, U. Fischer, M. Schwyzer, and P. Cumming, "Positronium lifetime validation measurements using a long-axial field-of-view positron emission tomography scanner," *EJNMMI Physics*, vol. 11, no. 1, p. 76, 2024. [Online]. Available: <https://doi.org/10.1186/s40658-024-00678-4>
- [7] L. Mercolli, W. M. Steinberger, H. Sari, A. Afshar-Oromieh, F. Caobelli, M. Conti, Á. R. Felgosa Cardoso, C. Mingels, P. Moskal, T. Pyka, N. Rathod, R. Schepers, R. Seifert, K. Shi, E. Ł. Stępień, M. Viscione, and A. O. Rominger, "In Vivo Positronium Lifetime Measurements with a Long Axial Field-of-View PET/CT," *medRxiv*, 2024. [Online]. Available: <https://www.medrxiv.org/content/early/2024/10/22/2024.10.19.24315509>
- [8] P. Moskal, D. Kisiełewska, R. Y. Shopa, Z. Bura, J. Chhokar, C. Curceanu, E. Czerwiński, M. Dadgar, K. Dulski, J. Gajewski, A. Gajos, M. Gorgol, R. Del Grande, B. C. Hiesmayr, B. Jasińska, K. Kacprzak, A. Kaminska, L. Kaplon, H. Karimi, G. Korcyl, P. Kowalski, N. Krawczyk, W. Krzemień, T. Kozik, E. Kubicz, P. Małczak, M. Mohammed, S. Niedźwiecki, M. Palka, M. Pawlik-Niedźwiecka, M. Pedziwiatr, L. Raczynski, J. Raj, A. Rucinski, S. Sharma, S. Shivani, M. Silarski, M. Skurzok, E. Ł. Stępień, S. Vandenberghe, W. Wiślicki, and B. Zgardzińska, "Performance assessment of the  $2\gamma$  positronium imaging with the total-body PET scanners," *EJNMMI Phys.*, vol. 7, p. 44, 2020.
- [9] T. Ahn, D. W. Gidley, A. W. Thornton, A. G. Wong-Foy, B. G. Orr, K. M. Kozloff, and M. M. Banaszak Holl, "Hierarchical nature of nanoscale porosity in bone revealed by positron annihilation lifetime spectroscopy," *ACS Nano*, vol. 15, p. 4321, 2021.
- [10] P. Moskal, K. Dulski, N. Chug, C. Curceanu, E. Czerwiński, M. Dadgar, J. Gajewski, A. Gajos, G. Grudzień, B. C. Hiesmayr, K. Kacprzak, Ł. Kaplon, H. Karimi, K. Klimaszewski, G. Korcyl, P. Kowalski, T. Kozik, N. Krawczyk, W. Krzemień, E. Kubicz, P. Małczak, S. Niedźwiecki, M. Pawlik-Niedźwiecka, M. Pędziwiatr, L. Raczynski, J. Raj, A. Rucinski, S. Sharma, S. null, R. Y. Shopa, M. Silarski, M. Skurzok, E. Ł. Stępień, M. Szczepanek, F. Tayefi, and W. Wiślicki, "Positronium imaging with the novel multiphoton PET scanner," *Science Advances*, vol. 7, no. 42, p. eabh4394, 2021.
- [11] Y. Jean, Y. Li, G. Liu, H. Chen, Z. J., and J. Gadzia, "Applications of slow positrons to cancer research: Search for selectivity of positron annihilation to skin cancer," *Applied Surface Science*, vol. 252, p. 3166, 2006.
- [12] H. Chen, J. van Horn, and Y. Jean, "Applications of positron annihilation spectroscopy to life science," *Defect Diffusion Forum*, vol. 331, p. 275, 2012.
- [13] B. Jasińska, B. Zgardzińska, G. Chołubek, M. Gorgol, K. Wiktor, K. Wysogład, P. Białas, C. Curceanu, E. Czerwiński, K. Dulski, A. Gajos, B. Głowacz, B. Hiesmayr, B. Jodłowska-Jędrych, D. Kamińska, G. Korcyl, P. Kowalski, T. Kozik, N. Krawczyk, W. Krzemień, E. Kubicz, M. Mohammed, M. Pawlik-Niedźwiecka, S. Niedźwiecki, M. Palka, L. Raczynski, Z. Rudy, N. Sharma, S. Sharma, R. Shopa, M. Silarski, M. Skurzok, A. Wiecek, H. Wiktor, W. Wiślicki, M. Zieliński, and P. Moskal, "Human tissues investigation using pals technique," *Acta Phys. Polon. B*, vol. 48, p. 1737, 2017.
- [14] B. Zgardzińska, G. Chołubek, B. Jarosz, K. Wysogład, M. Gorgol, M. Goździuk, M. Chołubek, and B. Jasińska, "Studies on healthy and neoplastic tissues using positron annihilation lifetime spectroscopy and focused histopathological imaging," *Sci. Rep.*, vol. 10, p. 11890, 2020.
- [15] H. Karimi, P. Moskal, A. Zak, and E. Stępień, "3d melanoma spheroid model for the development of positronium biomarker," *Sci. Rep.*, vol. 13, p. 1648, 2023.
- [16] P. Moskal, E. Kubicz, G. Grudzień, E. Czerwiński, K. Dulski, B. Leszczyński, S. Niedźwiecki, and E. Ł. Stępień, "Developing a novel positronium biomarker for cardiac myxoma imaging," *EJNMMI Physics*, vol. 10, no. 1, p. 22, 2023.
- [17] S. Moyo, P. Moskal, and E. Ł. Stępień, "Feasibility study of positronium application for blood clots structural characteristics," *Bio-Algorithms and Med-Systems*, vol. 18, no. 1, pp. 163–167, 12 2022. [Online]. Available: <http://dx.doi.org/10.2478/bioal-2022-0087>
- [18] S. Bass, S. Mariazzi, P. Moskal, and E. Stępień, "Positronium physics and biomedical applications," *Rev. Mod. Phys.*, vol. 95, p. 021002, 2023.
- [19] Y. C. Jean, P. E. Mallon, and D. M. Schrader, Eds., *Principles and Applications of Positron and Positronium Chemistry*, ser. Advanced Series in Physical Chemistry. World Scientific, 2003, vol. 12.
- [20] D. W. Gidley, H.-G. Peng, and R. S. Vallery, "Positron annihilation as a method to characterize porous materials," *Annual Review of Materials Research*, vol. 36, no. Volume 36, 2006, pp. 49–79, 2006. [Online]. Available: <https://www.annualreviews.org/content/journals/10.1146/annurev.matsci.36.111904.135144>
- [21] P. Moskal, D. Kisiełewska, C. Curceanu, E. Czerwiński, K. Dulski, A. Gajos, M. Gorgol, B. Hiesmayr, B. Jasińska, K. Kacprzak, Ł. Kaplon, G. Korcyl, P. Kowalski, W. Krzemień, T. Kozik, E. Kubicz, M. Mohammed, S. Niedźwiecki, M. Palka, M. Pawlik-Niedźwiecka, L. Raczynski, J. Raj, S. Sharma, Shivani, R. Y. Shopa, M. Silarski, M. Skurzok, E. Stępień, W. Wiślicki, and B. Zgardzińska, "Feasibility study of the positronium imaging with the J-PET tomograph," *Phys. Med. Biol.*, vol. 64, no. 5, p. 055017, 2019.
- [22] J. Qi and B. Huang, "Positronium lifetime image reconstruction for TOF PET," *IEEE Transactions on Medical Imaging*, vol. 41, p. 2848, 2022.
- [23] B. Huang, T. Li, G. Ariño-Estrada, K. Dulski, R. Y. Shopa, P. Moskal, E. Stępień, and J. Qi, "SPLIT: Statistical positronium lifetime image reconstruction via time-thresholding," *IEEE Transactions on Medical Imaging*, pp. 1–1, 2024.
- [24] B. Huang, Z. Wang, X. Zeng, A. H. Goldan, and J. Qi, "Fast high-resolution lifetime image reconstruction for positron lifetime tomography," *Communications Physics*, vol. 8, no. 1, 4 2025. [Online]. Available: <http://dx.doi.org/10.1038/s42005-025-02100-6>
- [25] H.-H. Huang, Z. Zhu, S. Boopasiri, Z. Chen, S. Pang, and C.-M. Kao, "A Statistical Reconstruction Algorithm for Positronium Lifetime Imaging Using Time-of-Flight Positron Emission Tomography," *IEEE Transactions on Radiation and Plasma Medical Sciences*, vol. 9, no. 4, pp. 478–486, 4 2025. [Online]. Available: <http://dx.doi.org/10.1109/trpms.2025.3531225>
- [26] M. Das, W. Mryka, E. Yitayew, S. Parzych, S. Sharma, E. Stępień, and P. Moskal, "Estimating the efficiency and purity for detecting annihilation and prompt photons for positronium imaging with J-PET using toy monte carlo simulation," *Bio-Algorithms and Med-Systems*, vol. 19, pp. 87–95, 2023.
- [27] K. Shibuya, H. Saito, F. Nishikido, M. Takahashi, and T. Yamaya, "Oxygen sensing ability of positronium atom for tumor hypoxia imaging," *Commun. Phys.*, vol. 3, p. 173, 2020.
- [28] P. Moskal and E. Stępień, "Perspectives on translation of positronium imaging into clinics," *Frontiers in Physics*, vol. 10, 2022.
- [29] K. Shibuya, H. Saito, H. Tashima, and T. Yamaya, "Using inverse laplace transform in positronium lifetime imaging," *Physics in Medicine and Biology*, vol. 67, p. 025009, 2022.
- [30] S. Takyu, K.-i. Matsumoto, T. Hirade, F. Nishikido, G. Akamatsu, H. Tashima, M. Takahashi, and T. Yamaya, "Quantification of radicals in aqueous solution by positronium lifetime: an experiment using a clinical PET scanner," *Japanese Journal of Applied Physics*, vol. 63, no. 8, p. 086003, aug 2024. [Online]. Available: <https://dx.doi.org/10.35848/1347-4065/ad679a>
- [31] S. Takyu, F. Nishikido, H. Tashima, G. Akamatsu, K. ichiro Matsumoto, M. Takahashi, and T. Yamaya, "Positronium lifetime measurement using a clinical PET system for tumor hypoxia identification," *Nuclear Instruments and Methods in Physics Research Section A: Accelerators, Spectrometers, Detectors and Associated Equipment*, vol. 1065, p. 169514, 2024. [Online]. Available: <https://www.sciencedirect.com/science/article/pii/S0168900224004406>
- [32] B. Huang, B. Dai, E. J. Li, J. S. Karp, and J. Qi, "High-resolution Positronium Lifetime Imaging on the PennPET Explorer," in *2024 IEEE Nuclear Science Symposium (NSS), Medical Imaging Conference (MIC) and Room Temperature Semiconductor Detector Conference (RTSD)*, 2024, pp. 1–1.
- [33] P. Moskal, A. Gajos, M. Mohammed, J. Chhokar, N. Chug, C. Curceanu, E. Czerwiński, M. Dadgar, K. Dulski, M. Gorgol, J. Goworek, B. C. Hiesmayr, B. Jasińska, K. Kacprzak, Ł. Kaplon, H. Karimi, D. Kisiełewska, K. Klimaszewski, G. Korcyl, P. Kowalski, N. Krawczyk, W. Krzemień, T. Kozik, E. Kubicz, S. Niedźwiecki, S. Parzych, M. Pawlik-Niedźwiecka, L. Raczynski, J. Raj, S. Sharma, S. Choudhary, R. Y. Shopa, A. Sienkiewicz, M. Silarski, M. Skurzok, E. Ł. Stępień, F. Tayefi, and W. Wiślicki, "Testing CPT symmetry in ortho-positronium decays with positronium annihilation tomography," *Nature Communications*, vol. 12, no. 1, 9 2021. [Online]. Available: <http://dx.doi.org/10.1038/s41467-021-25905-9>
- [34] P. Moskal, D. Kumar, S. Sharma, E. Y. Beyene, N. Chug, A. Coussat, C. Curceanu, E. Czerwiński, M. Das, K. Dulski, M. Gorgol, B. Jasińska, K. Kacprzak, T. Kaplanoglu, Ł. Kaplon, T. Kozik, E. Lisowski, F. Lisowski, W. Mryka, S. Niedźwiecki, S. Parzych, E. P. del Rio, M. Rädler, M. Skurzok, E. Ł. Stępień, P. Tanty, K. T. Ardebili, and K. V. Eliyan, "Nonmaximal entanglement of photons

- from positron-electron annihilation demonstrated using a plastic PET scanner," *Science Advances*, vol. 11, no. 18, 5 2025. [Online]. Available: <http://dx.doi.org/10.1126/sciadv.ads3046>
- [35] P. Moskal, E. Czerwiński, J. Raj, S. D. Bass, E. Y. Beyene, N. Chug, A. Coussat, C. Curceanu, M. Dadgar, M. Das, K. Dulski, A. Gajos, M. Gorgol, B. C. Hiesmayr, B. Jasińska, K. Kacprzak, T. Kaplanoglu, L. Kaplon, K. Klimaszewski, P. Konieczka, G. Korcyl, T. Kozik, W. Krzemień, D. Kumar, S. Moyo, W. Mryka, S. Niedźwiecki, S. Parzych, E. P. del Río, L. Raczynski, S. Sharma, S. Choudhary, R. Y. Shopa, M. Silarski, M. Kurzok, E. Ł. Stepień, P. Tanty, F. T. Ardebili, K. T. Ardebili, K. V. Eliyan, and W. Wislicki, "Discrete symmetries tested at 10–4 precision using linear polarization of photons from positronium annihilations," *Nature Communications*, vol. 15, no. 1, 1 2024. [Online]. Available: <http://dx.doi.org/10.1038/s41467-023-44340-6>
- [36] J. T. Triffitt and W. F. Neuman, "The uptake of sodium-22 by bone and certain soft tissues," *Calcified Tissue Research*, vol. 6, no. 1, pp. 70–76, 12 1970. [Online]. Available: <http://dx.doi.org/10.1007/BF02196185>
- [37] M. Sitarz, J.-P. Cussonneau, T. Matulewicz, and H. F., "Radionuclide candidates for for  $\beta^+\gamma$  coincidence PET: An overview," *Applied Radiation and Isotopes*, vol. 155, p. 108898, 2020.
- [38] P. Moskal and E. Ł. Stepień, "Prospects and clinical perspectives of total-body PET imaging using plastic scintillators," *PET Clinics*, vol. 15, pp. 439–452, 2020.
- [39] M. T. Durán, F. Juget, Y. Nedjadi, C. Bailat, P. V. Grundler, Z. Talip, N. P. van der Meulen, P. Casolaro, G. Dellepiane, and S. Braccini, "Half-life measurement of  $^{44}\text{Sc}$  and  $^{44\text{m}}\text{Sc}$ ," *Applied Radiation and Isotopes*, vol. 190, p. 110507, 12 2022. [Online]. Available: <http://dx.doi.org/10.1016/j.apradiso.2022.110507>
- [40] K. A. Domnanich, C. Müller, R. Farkas, R. M. Schmid, B. Ponsard, R. Schibli, A. Türler, and N. P. van der Meulen, " $^{44}\text{Sc}$  for labeling of DOTA- and NODAGA-functionalized peptides: preclinical in vitro and in vivo investigations," *EJNMMI Radiopharmacy and Chemistry*, vol. 1, no. 1, 5 2016. [Online]. Available: <http://dx.doi.org/10.1186/s41181-016-0013-5>
- [41] E. Koumariou, N. Loktionova, M. Fellner, F. Roesch, O. Thews, D. Pawlak, S. Archimandritis, and R. Mikolajczak, " $^{44}\text{Sc}$ -DOTA-BN[2-14]NH<sub>2</sub> in comparison to  $^{68}\text{Ga}$ -DOTA-BN[2-14]NH<sub>2</sub> in pre-clinical investigation. Is  $^{44}\text{Sc}$  a potential radionuclide for PET?" *Applied Radiation and Isotopes*, vol. 70, no. 12, pp. 2669–2676, 12 2012. [Online]. Available: <http://dx.doi.org/10.1016/j.apradiso.2012.08.004>
- [42] C. Müller, M. Bunka, J. Reber, C. Fischer, K. Zhernosekov, A. Türler, and R. Schibli, "Promises of Cyclotron-Produced  $^{44}\text{Sc}$  as a Diagnostic Match for Trivalent  $\beta^-$ -Emitters: In Vitro and In Vivo Study of a  $^{44}\text{Sc}$ -DOTA-Folate Conjugate," *Journal of Nuclear Medicine*, vol. 54, no. 12, pp. 2168–2174, 2013. [Online]. Available: <http://dx.doi.org/10.2967/jnumed.113.123810>
- [43] S. Eigner, D. R. B. Vera, M. Fellner, N. S. Loktionova, M. Piel, O. Lebeda, F. Rösch, T. L. Roß, and K. E. Henke, "Imaging of Protein Synthesis: In Vitro and In Vivo Evaluation of  $^{44}\text{Sc}$ -DOTA-Puromycin," *Molecular Imaging and Biology*, vol. 15, no. 1, pp. 79–86, 5 2012. [Online]. Available: <http://dx.doi.org/10.1007/s11307-012-0561-3>
- [44] R. Hernandez, H. F. Valdovinos, Y. Yang, R. Chakravarty, H. Hong, T. E. Barnhart, and W. Cai, " $^{44}\text{Sc}$ : An Attractive Isotope for Peptide-Based PET Imaging," *Molecular Pharmaceutics*, vol. 11, no. 8, pp. 2954–2961, 7 2014. [Online]. Available: <http://dx.doi.org/10.1021/mp500343j>
- [45] R. Chakravarty, S. Goel, H. F. Valdovinos, R. Hernandez, H. Hong, R. J. Nickles, and W. Cai, "Matching the Decay Half-Life with the Biological Half-Life: ImmunoPET Imaging with  $^{44}\text{Sc}$ -Labeled Cetuximab Fab Fragment," *Bioconjugate Chemistry*, vol. 25, no. 12, pp. 2197–2204, 11 2014. [Online]. Available: <http://dx.doi.org/10.1021/bc500415x>
- [46] D. Szücs, T. Csupász, J. P. Szabó, A. Kis, B. Gyuricza, V. Arató, V. Forgács, A. Vágner, G. Nagy, I. Garai, D. Szikra, I. Tóth, G. Trencsényi, G. Tircsó, and A. Fekete, "Synthesis, Physicochemical, Labeling and In Vivo Characterization of  $^{44}\text{Sc}$ -Labeled DO3AM-NI as a Hypoxia-Sensitive PET Probe," *Pharmaceuticals*, vol. 15, no. 6, p. 666, 5 2022. [Online]. Available: <http://dx.doi.org/10.3390/ph15060666>
- [47] A. Majkowska-Pilip and A. Bilewicz, "Macrocyclic complexes of scandium radionuclides as precursors for diagnostic and therapeutic radiopharmaceuticals," *Journal of Inorganic Biochemistry*, vol. 105, no. 2, pp. 313–320, 2 2011. [Online]. Available: <http://dx.doi.org/10.1016/j.jinorgbio.2010.11.003>
- [48] M. Pruszyński, A. Majkowska-Pilip, N. S. Loktionova, E. Eppard, and F. Roesch, "Radiolabeling of DOTATOC with the long-lived positron emitter  $^{44}\text{Sc}$ ," *Applied Radiation and Isotopes*, vol. 70, no. 6, pp. 974–979, 6 2012. [Online]. Available: <http://dx.doi.org/10.1016/j.apradiso.2012.03.005>
- [49] T. V. M. Lima, S. Gnesin, E. Nitzsche, P. G. Ortega, C. Müller, and N. P. van der Meulen, "First Phantom-Based Quantitative Assessment of Scandium-44 Using a Commercial PET Device," *Frontiers in Physics*, vol. 8, 7 2020. [Online]. Available: <http://dx.doi.org/10.3389/fphy.2020.00241>
- [50] T. V. M. Lima, S. Gnesin, K. Strobel, M. d. S. Pérez, J. E. Roos, C. Müller, and N. P. van der Meulen, "Fifty Shades of Scandium: Comparative Study of PET Capabilities Using Sc-43 and Sc-44 with Respect to Conventional Clinical Radionuclides," *Diagnostics*, vol. 11, no. 10, p. 1826, 10 2021. [Online]. Available: <http://dx.doi.org/10.3390/diagnostics11101826>
- [51] C. A. Umbricht, M. Benešová, R. M. Schmid, A. Türler, R. Schibli, N. P. van der Meulen, and C. Müller, " $^{44}\text{Sc}$ -PSMA-617 for radiotheragnostics in tandem with  $^{177}\text{Lu}$ -PSMA-617—preclinical investigations in comparison with  $^{68}\text{Ga}$ -PSMA-11 and  $^{68}\text{Ga}$ -PSMA-617," *EJNMMI Research*, vol. 7, no. 1, 1 2017. [Online]. Available: <http://dx.doi.org/10.1186/s13550-017-0257-4>
- [52] C. Müller, M. Bunka, S. Haller, U. Köster, V. Groehn, P. Bernhardt, N. van der Meulen, A. Türler, and R. Schibli, "Promising Prospects for  $^{44}\text{Sc}$ - $^{47}\text{Sc}$ -Based Theragnostics: Application of  $^{47}\text{Sc}$  for Radionuclide Tumor Therapy in Mice," *Journal of Nuclear Medicine*, vol. 55, no. 10, pp. 1658–1664, 7 2014. [Online]. Available: <http://dx.doi.org/10.2967/jnumed.114.141614>
- [53] J. Zhang, A. Singh, H. R. Kulkarni, C. Schuchardt, D. Müller, H.-J. Wester, T. Maina, F. Rösch, N. P. van der Meulen, C. Müller, H. Mäcke, and R. P. Baum, "From Bench to Bedside—The Bad Berka Experience With First-in-Human Studies," *Seminars in Nuclear Medicine*, vol. 49, no. 5, pp. 422–437, 9 2019. [Online]. Available: <http://dx.doi.org/10.1053/j.semnuclmed.2019.06.002>
- [54] E. Eppard, A. de la Fuente, M. Benešová, A. Khawar, R. A. Bundschuh, F. C. Gärtner, B. Kreppel, K. Kopka, M. Essler, and F. Rösch, "Clinical Translation and First In-Human Use of  $^{44}\text{Sc}$ -PSMA-617 for PET Imaging of Metastasized Castrate-Resistant Prostate Cancer," *Theranostics*, vol. 7, no. 18, pp. 4359–4369, 2017. [Online]. Available: <http://dx.doi.org/10.7150/thno.20586>
- [55] A. Singh, R. Baum, I. Klette, N. van der Meulen, C. Mueller, A. Tuerler, and R. Schibli, "Scandium-44 DOTATOC PET/CT: First in-human molecular imaging of neuroendocrine tumors and possible perspectives for Theragnostics," *Journal of Nuclear Medicine*, vol. 56, no. supplement 3, pp. 267–267, 2015. [Online]. Available: [https://jnm.snmjournals.org/content/56/supplement\\_3/267](https://jnm.snmjournals.org/content/56/supplement_3/267)
- [56] A. Khawar, E. Eppard, J. P. Sinnes, F. Roesch, H. Ahmadzadehfhar, S. Kürpig, M. Meisenheimer, F. C. Gaertner, M. Essler, and R. A. Bundschuh, " $^{44}\text{Sc}$ -PSMA-617 Biodistribution and Dosimetry in Patients With Metastatic Castration-Resistant Prostate Carcinoma," *Clinical Nuclear Medicine*, vol. 43, no. 5, pp. 323–330, 5 2018. [Online]. Available: <http://dx.doi.org/10.1097/rlu.0000000000002003>
- [57] N. P. van der Meulen, R. Hasler, Z. Talip, P. V. Grundler, C. Favaretto, C. A. Umbricht, C. Müller, G. Dellepiane, T. S. Carzaniga, and S. Braccini, "Developments toward the Implementation of  $^{44}\text{Sc}$  Production at a Medical Cyclotron," *Molecules*, vol. 25, no. 20, p. 4706, 10 2020. [Online]. Available: <http://dx.doi.org/10.3390/molecules25204706>
- [58] G. A. Prenosil, H. Sari, M. Fürstner, A. Afshar-Oromieh, K. Shi, A. Rominger, and M. Hentschel, "Performance characteristics of the biograph vision Quadra PET/CT system with a long axial field of view using the NEMA NU 2-2018 standard," *J. Nucl. Med.*, vol. 63, p. 476, 2022.
- [59] B. Dai, M. Daube-Witherspoon, S. McDonald, M. Werner, M. Parma, M. Geagan, V. Viswanath, and J. Karp, "Performance evaluation of the PennPET explorer with expanded axial coverage," *Phys. Med. Biol.*, vol. 68, p. 095007, 2023.
- [60] J. S. Karp, V. Viswanath, M. J. Geagan, G. Muehllehner, A. R. Pantel, M. J. Parma, A. E. Perkins, J. P. Schmall, M. E. Werner, and M. E. Daube-Witherspoon, "PennPET Explorer: Design and Preliminary Performance of a Whole-Body Imager," *Journal of Nuclear Medicine*, vol. 61, no. 1, pp. 136–143, 2020. [Online]. Available: <https://jnm.snmjournals.org/content/61/1/136>
- [61] B. Huang and J. Qi, "High-resolution positronium lifetime tomography by the method of moments," *Physics in Medicine & Biology*, vol. 69, no. 24, p. 24NT01, 12 2024. [Online]. Available: <http://dx.doi.org/10.1088/1361-6560/ad9543>
- [62] L. Berens, I. Hsu, C.-T. Chen, H. Halpern, and C.-M. Kao, "An analytic, moment-based method to estimate orthopositronium lifetimes in positron annihilation lifetime spectroscopy measurements," *Bio-Algorithms and Med-Systems*, vol. 20, no. Special Issue, pp. 40–48, 12 2024. [Online]. Available: <http://dx.doi.org/10.5604/01.3001.0054.9141>

- [63] Z. Chen, L. An, C.-M. Kao, and H.-H. Huang, "The properties of the positronium lifetime image reconstruction based on maximum likelihood estimation," *Bio-Algorithms and Med-Systems*, vol. 19, no. 1, pp. 1–8, 12 2023. [Online]. Available: <http://dx.doi.org/10.5604/01.3001.0054.1807>
- [64] R. Shopa and K. Dulski, "Positronium imaging in J-PET with an iterative activity reconstruction and a multi-stage fitting algorithm," *Bio-Algorithms and Med-Systems*, vol. 19, no. 1, pp. 54–63, 2023.
- [65] Z. Chen, C.-M. Kao, H.-H. Huang, and L. An, "Enhanced positronium lifetime imaging through two-component reconstruction in time-of-flight positron emission tomography," *Frontiers in Physics*, vol. 12, 7 2024. [Online]. Available: <http://dx.doi.org/10.3389/fphy.2024.1429344>
- [66] F. Tayefi Ardebili, S. Niedźwiecki, and P. Moskal, "Evaluation of Modular J-PET sensitivity," *Bio-Algorithms and Med-Systems*, vol. 19, p. 132, 2023.
- [67] F. Tayefi Ardebili and P. Moskal, "Assessing the Spatial Resolution of the Modular J-PET Scanner using the Maximum-Likelihood Expectation-Maximization (MLEM) algorithm," *Bio-Algorithms and Med-Systems*, vol. 20, no. Special Issue, pp. 1–9, 11 2024. [Online]. Available: <http://dx.doi.org/10.5604/01.3001.0054.8095>
- [68] S. Sharma, J. Chhokar, C. Curceanu, E. Czerwiński, M. Dadgar, K. Dulski, J. Gajewski, A. Gajos, M. Gorgol, N. Gupta-Sharma, R. D. Grande, B. C. Hiesmayr, B. Jasińska, K. Kacprzak, Ł. Kapłon, H. Karimi, D. Kisiełewska, K. Klimaszewski, G. Korcyl, P. Kowalski, T. Kozik, N. Krawczyk, W. Krzemień, E. Kubicz, M. Mohammed, S. Niedźwiecki, M. Pałka, M. Pawlik-Niedźwiecka, L. Raczynski, J. Raj, A. Ruciński, Shivani, R. Y. Shopa, M. Silarski, M. Skurczok, E. Ł. Stepień, W. Wiślicki, B. Zgardzińska, and P. Moskal, "Estimating relationship between the Time Over Threshold and energy loss by photons in plastic scintillators used in the J-PET scanner," *EJNMMI Phys.*, vol. 7, p. 39, 2020.
- [69] E. Y. Beyene, M. Das, M. Durak-Kozica, G. Korcyl, W. Mryka, S. Niedźwiecki, S. Parzych, K. Tayefi, R. Walczak, K. Wawrowicz, E. Stepień, and P. Moskal, "Exploration of simultaneous dual-isotope imaging with multiphoton modular J-PET scanner," *Bio-Algorithms and Med-Systems*, vol. 19, no. 1, pp. 101–108, 12 2023. [Online]. Available: <http://dx.doi.org/10.5604/01.3001.0054.1940>
- [70] A. Stolarz, J. A. Kowalska, J. Jastrzębski, J. Choiński, M. Sitarz, K. Szkliniarz, A. Trzcinańska, and W. Zipper, "Ca targets for sc production by proton or deuteron irradiation," *HIL Annual Report*, p. 30, 2016. [Online]. Available: [www.slj.uw.edu.pl](http://www.slj.uw.edu.pl)
- [71] A. Stolarz, J. A. Kowalska, J. Jastrzębski, J. Choiński, M. Sitarz, K. Szkliniarz, A. Trzcinańska, and W. Zipper, "Targets for production of the medical radioisotopes with alpha and proton or deuteron beams," *AIP Conference Proceedings*, vol. 2018, p. 020004, 2018.
- [72] J. Choiński and M. Łyczko, "Prospects for the production of radioisotopes and radiobioconjugates for theranostics," *Bio-Algorithms and Med-Systems*, vol. 17, p. 241, 2021.
- [73] S. Niedźwiecki, P. Białas, C. Curceanu, E. Czerwiński, K. Dulski, A. Gajos, B. Głowacz, M. Gorgol, B. C. Hiesmayr, B. Jasińska, Ł. Kapłon, D. Kisiełewska-Kamińska, G. Korcyl, P. Kowalski, T. Kozik, N. Krawczyk, W. Krzemień, E. Kubicz, M. Mohammed, M. Pawlik-Niedźwiecka, M. Pałka, L. Raczynski, Z. Rudy, N. G. Sharma, S. Sharma, R. Y. Shopa, M. Silarski, M. Skurczok, A. Wieczorek, W. Wiślicki, B. Zgardzińska, M. Zieliński, and P. Moskal, "J-PET: a new technology for the whole-body PET imaging," *Acta Phys. Polon. B*, vol. 48, p. 1567, 2017.
- [74] G. Korcyl, P. Białas, C. Curceanu, E. Czerwiński, K. Dulski, B. Flak, A. Gajos, B. Głowacz, M. Gorgol, B. C. Hiesmayr, B. Jasińska, K. Kacprzak, M. Kajetanowicz, D. Kisiełewska, P. Kowalski, T. Kozik, N. Krawczyk, W. Krzemień, E. Kubicz, M. Mohammed, S. Niedźwiecki, M. Pawlik-Niedźwiecka, M. Pałka, L. Raczynski, P. Rajda, Z. Rudy, P. Salabura, N. G. Sharma, S. Sharma, R. Y. Shopa, M. Skurczok, M. Silarski, P. Strzempek, A. Wieczorek, W. Wiślicki, R. Zaleski, B. Zgardzińska, M. Zieliński, and P. Moskal, "Evaluation of single-chip, real-time tomographic data processing on fpga soc devices," *IEEE Transactions on Medical Imaging*, vol. 37, no. 11, pp. 2526–2535, 2018.
- [75] P. Moskal, S. Niedźwiecki, T. Bednarski, E. Czerwiński, Ł. Kapłon, E. Kubicz, I. Moskal, M. Pawlik-Niedźwiecka, N. Sharma, M. Silarski, M. Zieliński, N. Zoń, P. Białas, A. Gajos, A. Kochanowski, G. Korcyl, J. Kowal, P. Kowalski, T. Kozik, W. Krzemień, M. Molenda, M. Pałka, L. Raczynski, Z. Rudy, P. Salabura, A. Słomski, J. Smyrski, A. Strzelecki, A. Wieczorek, and W. Wiślicki, "Test of a single module of the J-PET scanner based on plastic scintillators," *Nucl. Instr. and Meth. A*, vol. 764, pp. 317–321, 2014.
- [76] M. Das, R. Bayerlein, S. Sharma, S. Parzych, S. Niedźwiecki, R. Badawi, and E. Y. Beyene, "Development of correction techniques for the J-PET scanner," *Bio-Algorithms and Med-Systems*, vol. 20, no. 1, pp. 101–110, 2024. [Online]. Available: <https://doi.org/10.5604/01.3001.0054.9362>
- [77] T. Merlin, S. Stute, D. Benoit, J. Bert, T. Carlier, C. Comtat, M. Filipovic, F. Lamare, and D. Visvikis, "Castor: a generic data organization and processing code framework for multi-modal and multi-dimensional tomographic reconstruction," *Physics in Medicine & Biology*, vol. 63, no. 18, p. 185005, 2018.
- [78] K. Kotera, T. Saito, and T. Yamanaka, "Measurement of positron lifetime to probe the mixed molecular states of liquid water," *Physics Letters A*, vol. 345, no. 1, pp. 184–190, 2005. [Online]. Available: <https://www.sciencedirect.com/science/article/pii/S0375960105011035>
- [79] K. Dulski, B. Zgardzińska, P. Białas, C. Curceanu, E. Czerwiński, A. Gajos, B. Głowacz, M. Gorgol, B. C. Hiesmayr, B. Jasińska, D. Kisiełewska-Kamińska, G. Korcyl, P. Kowalski, T. Kozik, N. Krawczyk, W. Krzemień, E. Kubicz, M. Mohammed, M. P.-N. S. Niedźwiecki, M. Pałka, L. Raczynski, J. Raj, Z. Rudy, N. G. Sharma, S. Sharma, Shivani, R. Y. Shopa, M. Silarski, M. Skurczok, A. Wieczorek, W. Wiślicki, M. Zieliński, and P. Moskal, "Analysis procedure of the positronium lifetime spectra for the J-PET detector," *Acta Phys. Polon. A*, vol. 132, no. 5, pp. 1637–1640, 2017.
- [80] K. Dulski, C. Curceanu, E. Czerwiński, A. Gajos, M. Gorgol, N. Gupta-Sharma, B. C. Hiesmayr, B. Jasińska, K. Kacprzak, Ł. Kapłon, D. Kisiełewska, K. Klimaszewski, G. Korcyl, P. Kowalski, N. Krawczyk, W. Krzemień, T. Kozik, E. Kubicz, M. Mohammed, S. Niedźwiecki, M. Pałka, M. Pawlik-Niedźwiecka, L. Raczynski, J. Raj, K. Rakoczy, Z. Rudy, S. Sharma, Shivani, R. Y. Shopa, M. Silarski, M. Skurczok, W. Wiślicki, B. Zgardzińska, and P. Moskal, "Commissioning of the J-PET detector in view of the positron annihilation lifetime spectroscopy," *Hyperfine Interactions*, vol. 239, no. 1, p. 40, 2020.
- [81] K. Dulski, "PALS avalanche - a new PAL spectra analysis software," *Acta Phys. Polon. A*, vol. 137, no. 2, pp. 167–170, 2020.
- [82] H. F. Mohamed, A. El-Sayed, and G. G. Abd-ElSadek, "Effect of temperature on ortho-positronium in poly(methyl methacrylate)," *Polymer Degradation and Stability*, vol. 71, no. 1, pp. 93–97, 2000. [Online]. Available: <https://www.sciencedirect.com/science/article/pii/S0141391000001579>
- [83] Ł. Kapłon, J. Baran, N. Chug, A. Coussat, C. Curceanu, E. Czerwiński, M. Dadgar, K. Dulski, J. Gajewski, A. Gajos, B. Hiesmayr, E. K. Valsan, K. Klimaszewski, G. Korcyl, T. Kozik, W. Krzemień, D. Kumar, G. Moskal, S. Niedźwiecki, D. Panek, S. Parzych, E. P. del Rio, L. Raczynski, A. Ruciński, S. Sharma, S. Shivani, R. Shopa, M. Silarski, M. Skurczok, E. Stepień, F. T. Ardebili, K. T. Ardebili, W. Wiślicki, and P. Moskal, "Comparative studies of plastic scintillator strips with high technical attenuation length for the total-body J-PET scanner," *Nuclear Instruments and Methods in Physics Research Section A: Accelerators, Spectrometers, Detectors and Associated Equipment*, vol. 1051, p. 168186, 2023. [Online]. Available: <https://www.sciencedirect.com/science/article/pii/S0168900223001766>
- [84] P. Moskal, E. Stepień, and A. Khreptak, "A vision to increase the availability of PET diagnostics in low- and medium-income countries by combining a low-cost modular J-PET tomograph with the  $^{44}\text{Ti}/^{44}\text{Sc}$  generator," *Bio-Algorithms and Med-Systems*, vol. 20, no. Special Issue, pp. 55–62, 12 2024. [Online]. Available: <http://dx.doi.org/10.5604/01.3001.0054.9273>
- [85] C. V. Gomes, B. M. Mendes, L. Paixão, S. Gnesin, C. Müller, N. P. van der Meulen, K. Strobel, T. C. F. Fonseca, and T. V. M. Lima, "Comparison of the dosimetry of scandium-43 and scandium-44 patient organ doses in relation to commonly used gallium-68 for imaging neuroendocrine tumours," *EJNMMI Physics*, vol. 11, no. 1, 7 2024. [Online]. Available: <http://dx.doi.org/10.1186/s40658-024-00669-5>
- [86] P. Moskal, P. Kowalski, R. Shopa, L. Raczynski, J. Baran, N. Chug, C. Curceanu, E. Czerwiński, M. Dadgar, K. Dulski, A. Gajos, B. Hiesmayr, K. Kacprzak, Ł. Kapłon, D. Kisiełewska, K. Klimaszewski, P. Kopka, G. Korcyl, N. Krawczyk, W. Krzemień, E. Kubicz, S. Niedźwiecki, S. Parzych, J. Raj, S. Sharma, S. Shivani, E. Stepień, F. Tayefi, and W. Wiślicki, "Simulating NEMA characteristics of the modular total-body J-PET scanner — an economic total-body PET from plastic scintillators," *Phys. Med. Biol.*, vol. 66, p. 175015, 2021.
- [87] B. A. Spencer, E. Berg, J. P. Schmall, N. Omidvari, E. K. Leung, Y. G. Abdelhafez, S. Tang, Z. Deng, Y. Dong, Y. Lv, J. Bao, W. Liu, H. Li, T. Jones, R. D. Badawi, and S. R. Cherry, "Performance evaluation of the uEXPLORER total-body PET/CT scanner based on NEMA NU 2-2018 with additional tests to characterize PET scanners with a long axial field of view," *J. Nucl. Med.*, vol. 61, p. 861, 2021.